



City Research Online

City, University of London Institutional Repository

Citation: Jawaid, M. M., Narejo, S., Riaz, F., Reyes-Aldasoro, C. C., Slabaugh, G. & Brown, J. (2024). Non-calcified plaque-based coronary stenosis grading in contrast enhanced CT. *Medical Engineering & Physics*, 129, 104182. doi: 10.1016/j.medengphy.2024.104182

This is the published version of the paper.

This version of the publication may differ from the final published version.

Permanent repository link: <https://openaccess.city.ac.uk/id/eprint/33040/>

Link to published version: <https://doi.org/10.1016/j.medengphy.2024.104182>

Copyright: City Research Online aims to make research outputs of City, University of London available to a wider audience. Copyright and Moral Rights remain with the author(s) and/or copyright holders. URLs from City Research Online may be freely distributed and linked to.

Reuse: Copies of full items can be used for personal research or study, educational, or not-for-profit purposes without prior permission or charge. Provided that the authors, title and full bibliographic details are credited, a hyperlink and/or URL is given for the original metadata page and the content is not changed in any way.

City Research Online:

<http://openaccess.city.ac.uk/>

publications@city.ac.uk



Paper



Non-calcified plaque-based coronary stenosis grading in contrast enhanced CT

Muhammad Moazzam Jawaid^{a,*}, Sanam Narejo^d, Farhan Riaz^a,
Constantino Carlos Reyes-Aldasoro^b, Greg Slabaugh^c, James Brown^a

^a University of Lincoln, UK

^b City, University of London, UK

^c Queen Mary University of London, UK

^d Mehran University of Engineering and Technology, Jamshoro, Pakistan

ARTICLE INFO

Keywords:

Coronary stenosis

CNN

Non-calcified plaque

Plaque quantification

Inter-observer variations

ABSTRACT

Background: The high mortality rate associated with coronary heart disease has led to state-of-the-art non-invasive methods for cardiac diagnosis including computed tomography and magnetic resonance imaging. However, stenosis computation and clinical assessment of non-calcified plaques has been very challenging due to their ambiguous intensity response in CT i.e. a significant overlap with surrounding muscle tissues and blood. Accordingly, this research presents an approach for computation of coronary stenosis by investigating cross-sectional lumen behaviour along the length of 3D coronary segments.

Methods: Non-calcified plaques are characterized by comparatively lower-intensity values with respect to the surrounding. Accordingly, segment-wise orthogonal volume was reconstructed in 3D space using the segmented coronary tree. Subsequently, the cross sectional volumetric data was investigated using proposed CNN-based plaque quantification model and subsequent stenosis grading in clinical context was performed. In the last step, plaque-affected orthogonal volume was further investigated by comparing vessel-wall thickness and lumen area obstruction w.r.t. expert-based annotations to validate the stenosis grading performance of model.

Results: The experimental data consists of clinical CT images obtained from the Rotterdam CT repository leading to 600 coronary segments and subsequent 15786 cross-sectional images. According to the results, the proposed method quantified coronary vessel stenosis i.e. severity of the non-calcified plaque with an overall accuracy of 83%. Moreover, for individual grading, the proposed model show promising results with accuracy equal to 86%, 90% and 79% respectively for severe, moderate and mild stenosis. The stenosis grading performance of the proposed model was further validated by performing lumen-area versus wall-thickness analysis as per annotations of manual experts. The statistical results for lumen area analysis precisely correlates with the quantification performance of the model with a mean deviation of 5% only.

Conclusion: The overall results demonstrates capability of the proposed model to grade the vessel stenosis with reasonable accuracy and precision equivalent to human experts.

1. Introduction

In a clinical context, the term Coronary Heart Disease (CHD) refers to deposition of cholesterol and related fatty materials (plaque) at different locations inside coronary tree. Gradually with the passage of time, this plaque buildup starts causing obstruction (stenosis) to the

blood flow towards heart muscles. As a result, oxygen-starved heart muscles result in adverse cardiac events including Congestive Heart Failure, Angina and Arrhythmias. According to the global heart diseases fact-sheet released by British Heart Foundation [1], a substantial number of around 620 million people are suffering with coronary and circulatory diseases around the globe and this number is continuously

* Corresponding author.

E-mail addresses: mjawaid@lincoln.ac.uk (M.M. Jawaid), sanam.narejo@faculty.muett.edu.pk (S. Narejo), friaz@lincoln.ac.uk (F. Riaz), constantino-carlos.reyes-aldasoro@city.ac.uk (C.C. Reyes-Aldasoro), greg.slabaugh@city.ac.uk (G. Slabaugh), jamesbrown@lincoln.ac.uk (J. Brown).

<https://doi.org/10.1016/j.medengphy.2024.104182>

Received 13 February 2024; Received in revised form 8 April 2024; Accepted 17 May 2024

Available online 22 May 2024

1350-4533/© 2024 The Author(s). Published by Elsevier Ltd on behalf of IPREM. This is an open access article under the CC BY license (<http://creativecommons.org/licenses/by/4.0/>).

increasing due to changing lifestyles. As per statistics, there were an estimated 285 million affected people globally, which rose to 350 million in 2000, 430 million in 2010 and subsequently 550 million in 2019. Moreover, approximately 60 million people across the world develop coronary related disease annually i.e. equivalent to the entire population of the UK. The growing clinical threat related with CHD has resulted in revolutionary developments in medical imaging arena including sub-millimeter CT and MRI scanning. Based on high temporal and spatial resolution, these advancements are being used practically in health facilities and have overall improved the diagnostic accuracy [2]. These imaging protocols can certainly help clinicians in precise and early detection of arterial anomalies helping them to control and normalize the clinical threat [3].

Modern CT apparatus captures internal details with sub-millimeter accuracy and serves as a feasible alternative to complex catheterizing process for detecting obstruction [4]; however, the nature of the coronary plaques pose a formidable challenge in the precise diagnosis. The hard plaques or calcified plaques are easily traceable in CT due to the intensity response of Calcium and a number of works [5–8] have been reported in literature with a reasonable computation accuracy. On the other hand, cholesterol-based non-calcified plaques (NCP) exhibits comparatively lower intensity values (quite close to surrounding tissues) making quantification a challenging problem for research community.

It is important to mention that from clinical perspective, the vulnerable nature of the non-calcified plaques make them vital indicator of fatal coronary syndromes [9] as they are prone to sudden rupture as well as positive remodelling of vessels keep patient asymptomatic. The positive remodelling refers to the expansion of vessel-wall outwards i.e. the plaque present does not cause any narrowing symptoms. From clinical perspective, positive remodelling is very threatening as patient remain asymptomatic till sudden fatal event. Consequently, research community is interested to devise methods for early detection and overall plaque burden quantification i.e. computing degree of vessel stenosis to avoid worst cardiac events [10].

In context of paper organization, we start with a brief introduction followed by relevant literature in Section 2. In the subsequent section, we provide details about the CT dataset and ground truth construction to validate the outcomes of the proposed method. The next section presents an “inter-observer” variability analysis to demonstrate the fact that non-calcified plaque assessment is very challenging manually and there occurs significant “difference” among three experts evaluating same patient. This is followed by the methodology explaining segment-wise cross-sectional volume extraction followed by CNN application for stenosis grading computation. The result section then discusses the performance of classification model and validation of stenosis grading model by investigating lumen-area versus vessel-wall thickness graphical plots.

2. Related work

CTA-based Non-calcified plaque quantification and associated stenosis grading has been challenging problem; hence, a limited number of clinical studies have been reported in this context [11–14] mainly employing anomaly detection approach. The plaque quantification framework proposed by Clouse et al. [11] investigated manually selected 49 coronary segments (41 normal, 8 abnormal) to validate the proposed quantification method but the main motivation was to quantify the plaque amount from pre-extracted image planes. An extended version of this work was subsequently reported by [15] to correlate quantification capabilities of CT-imagery with intra-vascular ultrasound (IVUS) using 20 affected segments for comparative quantification. However, a notable limitation of this work was the manual identification of plaque lesions, hindering the implementation of an automated detection solution.

An interesting work employing Linear discriminant analysis (LDA) to detect non-calcified plaque was reported by Wei et al. [12]; however, the main focus was reduction of false-positive candidates in a set of 120 pre-selected soft plaque candidates. In an overall context, this work was focused on the detection of the non-calcified plaques rather than the precise quantification with reported detection accuracy of 92.5%. Likewise, Tessman et al. [14] proposed a method to quantify calcified and non-calcified plaques by extracting cylindrical volume around centreline but it lead to high false positives due to inclusion of surrounding muscles in the cylindrical space. Method proposed by Zuluaga et al. [16] employed machine learning for anomaly detection using manual intensity definitions and SVM. Although the accuracy 79.62% was reported for 9 clinical CTAs but conceptually quantification and grading was not performed. An interesting work in this context was reported by Athanasiou et al. i.e. [17] based upon 4-class Gaussian Mixture Model. The plaque labelled voxels were quantified and plaque volume was compared with IVUS segmentation for validation. The interesting finding of the work is that calcified plaque was quantified with good precision whereas blooming affect associated with non-calcified plaque led to decreased performance. In addition, a number of studies [18,19,15,20–23] have been reported However, these studies primarily aimed to showcase CTA imaging capabilities instead of automated stenosis computation. Hence, non-calcified plaque lesions were initially manually selected and the results of plaque quantification were then compared to intra-vascular ultrasound analysis to establish a correlation between the two imaging modalities.

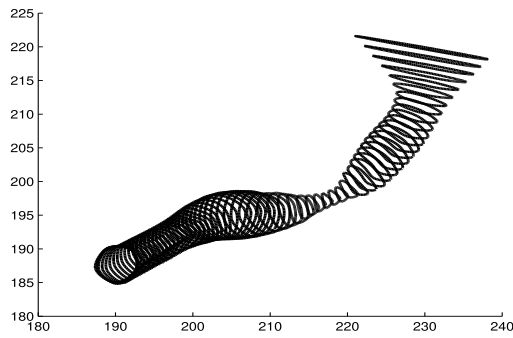
More recent works based upon Deep learning have been reported by Han et al. [24], Paul et al. [25] and Jin et al. [26] in this context; however, there have been associated limitations with reported literature respectively. For instance, propose method in [24] CCTA-AI facilitates plaque-associated images generation using a series of 2D CT images; however, this approach performs well for detecting regions where the stenosis goes beyond 50% and smaller instances are frequently missed. Similarly, [25] employs curved planer reformation to construct 2-D images from 3D CT which often leads to missing important information regarding vessel remodelling. Moreover, this work focused over occurrences of calcified plaques which has been reported quite frequently in literature. An interesting study by Jin et al. i.e. [26] employed 127,763 retrospective CT images for 505 patients from 5 medical centres. A CNN based methodology was used to perform coronary artery segmentation and subsequently perform plaque detection; however, it depends upon manually defined radiomics for precise plaque quantification and stenosis grading.

Our contribution in this work is an efficient method for coronary tree investigation and vessel stenosis grading with a human level of accuracy. Based on automated coronary segmentation method [27] vascular tree was extracted, followed by automated localization of non-calcified plaque in coronary segments. The 3D segmented coronary tree was then transformed into segment-wise cross-sectional volume followed by application of the customised CNN model for stenosis grading in respective segments. In the final step, we present an efficient method for the vessel wall analysis i.e. computation of vessel lumen area and plaque-related wall thickness to validate the results of stenosis classification.

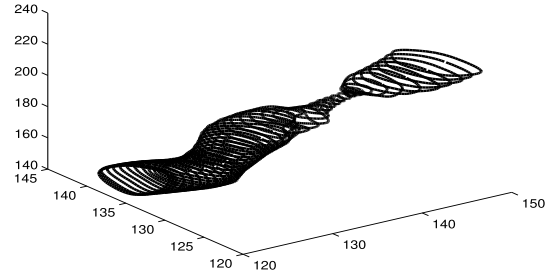
3. Clinical dataset acquisition

The clinical data investigated in this work consists of 20 CT volumes obtained from public resource i.e. anonymized CT dataset from Rotterdam Coronary Artery Evaluation framework [28,29]. The main reason for selecting Rotterdam CT dataset is provision of lumen reference-annotations for individual segments of coronary tree i.e. along with the CT image data for respective patients, human expert-based 3D boundary contours (both normal and plaque affected segments) are also provided for validation of results as shown in Fig. 1.

It is important to mention that 17-segment AHA coronary model is a standard reference model for clinical reporting and naturally there



(a) Lumen reduction in DS4Seg1



(b) Lumen reduction in DS7Seg2

Fig. 1. Boundary counters provided by manual experts of the Rotterdam coronary artery dataset for validation of results. (a-b) reflects the lumen contours i.e. manual annotation for two different plaque affected segments.

Table 1

Stenosis specifications for plaque affected segments.

Segment ID	Coronary Segment Specification				
	Segment	Grading	Length	Location	Stenosis(%)
DS1 seg6	Major	Mild	58	3-12	23
DS2 seg6	Major	Mild	67	25-42	25
DS4 seg1	Major	Severe	72	8-29	93
DS4 seg2	Major	Moderate	68	19-28	61
DS5 seg2	Major	Moderate	73	9-35	57
DS5 seg8	Minor	Moderate	42	2-22	55
DS7 seg2	Major	Severe	76	7-17	81
DS7 seg3	Major	Moderate	57	17-22	62
DS9 seg2	Major	Moderate	61	1-28	65
DS10 seg8	Minor	Moderate	42	13-56	55
DS11 seg7	Major	Mild	58	13-35	32
DS11 seg12	Minor	Mild	26	2-10	22
DS15 seg2	Major	Moderate	75	16-24	53
DS15 seg3	Major	Mild	59	8-15	35
DS15 seg14	Minor	Moderate	43	26-57	55

exists a wide inter-patient variability i.e. certain coronary segments do not exist for a specific patient. Moreover, out of the existing segments of the coronary tree, major/proximal segments are considered significant whereas minor/distal segments are given less importance. This is based on the fact that occlusion in a major segment can cause obstruction onwards to multiple branches leading to fatal consequences whereas minor segments will not cause hierarchical branch damage onwards. Accordingly, we identified the target segments from the Rotterdam CTA data i.e. the non-calcified plaque affected segments with associated lumen boundary demarcations (in terms of 3D discrete contours) as defined in the Table 1. Although the plaque position is precisely specified by manual experts in terms of compressed vessel boundary inside segment; however, it was observed visually that the presence of plaque leads to intensity drop phenomena throughout the length of the segment. Hence, all cross sections of plaque affected segment are considered as abnormal to compensate the intensity variations associate with internal obstruction.

In order to ensure that the meaningful training of the model, data augmentation was performed for non-calcified plaque associate cross sections. Accordingly, rotation, scale-variations, flip and shear operations were performed to create 8 copies for every affected image leading to a total sum of 7893 cross-sections. In addition to abnormal-cross sections, we also obtained “normal” cross sectional slices from healthy segments of coronary tree to ensure that CNN model should learn characteristics of healthy lumen while computing stenosis. Accordingly, same number of healthy cross-sections i.e. 7893 was selected to avoid any class-imbalance issues in later stage.

4. Vessel segmentation and ground truth formulation

4.1. Coronary tree segmentation

The first step towards vessel stenosis computation is precise segmentation of the coronary tree from the 3D CTA volume. Accordingly, automated coronary segmentation was performed to extract 3D coronary tree using hybrid energy methodology of [27]. Subsequently, we investigated respective coronary tree(s) for positioning plaques using method proposed in [30]. For reference, the extracted coronary tree for a particular patient is presented in Fig. 2a, with individual segments represented using three different colours.

4.2. Ground truth construction

In clinical practice, non-calcified plaque computation is done by computing shrinkage/deformation in vessel lumen indirectly [29] i.e. an approximation is made by comparing plaque region with healthy vessel behaviour as demonstrated in Fig. 1. For instance, the lumen diameter variations can be observed in the mid of the vessel from Fig. 1a - 1b indicating the presence of non-calcified plaque at respective locations. The conventional way of computing lumen stenosis percentage is to compute the cross-sectional diameter of vessel just before the beginning of the plaque and compare values with the plaque-affected cross sectional diameter. However, this leads to over estimation often by ignoring the fact that overall vessel diameter decreases along the length of the segment. Instead, we proposed to represent the complete segment using with a mathematical model T_{model} in first instance followed by precise computation of stenosis.

Accordingly, we used an elliptical tube model $T_{model} [CP, \theta'_{cs}]$ for segment approximation as it allows blood-flow and intra-lumen deformations. Here, CP denotes the centreline of the segment and θ'_{cs} defines the corresponding cross-section based boundary information for respective points of the centreline. Accordingly, the complete segment is approximated by $[N_s]$ by $[m]$ array as shown in Fig. 2b, where N_s represent the total number of points in the segment centreline and m denotes cross-section related parameters. For the i^{th} point of the centreline CP , we define the parameter vector $\theta'_{cs}(i)$ using an ellipse model as $[\{a(i), b(i), C_{xyz}(i), R_{xyz}(i)\} \approx E_{xyz}(i)]$, where $a(i)$ and $b(i)$ represent the lengths of the major and minor axes of the current ellipse, $C_{xyz}(i)$ denotes the centre of the i^{th} ellipse of segment, and $R_{xyz}(i)$ defines orientation information for i^{th} ellipse in 3D space.

The mathematical formulation (parametric representation) for a 3-dimensional ellipse is expressed by Eq. (1), where E_{xyz} denotes circumference of the ellipse, C_{xyz} is the centre of the ellipse, a, b represent the lengths of the major and minor axes, respectively, R_{xyz} denotes the orientation information of the ellipse in 3D space and t' is the angular

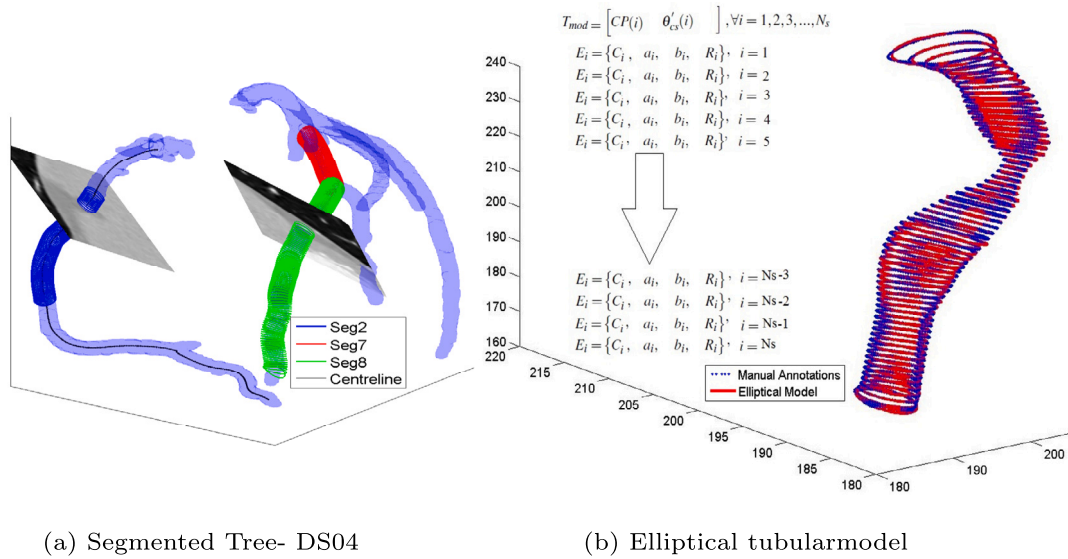


Fig. 2. Coronary tree (LCA and RCA) with overlaid skeleton and cross sectional planes. The centre-line is displayed in black colour whereas blue, red and green represents boundary contours for segments numbered 2, 7 and 8 respectively. (b) illustrates tubular model of the coronary segment. The successive boundary contours along the length of the segment are defined using elliptical approximations.

parameter varying between 0 to 2π . Moreover, the minimum distance of an arbitrary point, $P = [P_x, P_y, P_z]^T$ to the circumference of the ellipse can be found using Eq. (2).

$$E_{xyz} = \begin{bmatrix} C_x \\ C_y \\ C_z \end{bmatrix} + R_{xyz} \cdot \begin{bmatrix} a \cdot \cos(t') \\ b \cdot \sin(t') \\ 0 \end{bmatrix}, \quad \text{where, } R_{xyz} = R_1 R_2 R_3. \quad (1)$$

$$R1 = \begin{bmatrix} \cos(\alpha) & \sin(\alpha) & 0 \\ -\sin(\alpha) & \cos(\alpha) & 0 \\ 0 & 0 & 1 \end{bmatrix}, \quad R2 = \begin{bmatrix} 1 & 0 & 0 \\ 0 & \cos(\beta) & \sin(\beta) \\ 0 & -\sin(\beta) & \cos(\beta) \end{bmatrix},$$

$$R3 = \begin{bmatrix} \cos(\gamma) & \sin(\gamma) & 0 \\ -\sin(\gamma) & \cos(\gamma) & 0 \\ 0 & 0 & 1 \end{bmatrix}.$$

$$distt = \min_t |P - E_{xyz}|^2 = \left\| \begin{pmatrix} P_x \\ P_y \\ P_z \end{pmatrix} - \begin{pmatrix} C_x \\ C_y \\ C_z \end{pmatrix} - R_{xyz} \begin{pmatrix} a \cos(t') \\ b \sin(t') \\ 0 \end{pmatrix} \right\|^2. \quad (2)$$

For elliptical representation of the segment, we approximated manual demarcations using best fitting ellipses using non-linear least square fitting for respective cross sections of the coronary segment.

After obtaining the elliptical model of the vessel segment, we employed two “normal” ellipses adjacent to the lesion region i.e. (immediately before and after the plaque region) to derive the contours for ideal boundary i.e. stenosis-free vessel through the affected region as illustrated in Fig. 3. It is important to mention that “ideal” vessel boundary at “ith” point of the centreline was derived using local orientation information to precisely follow the progression of vessel in 3D space. However, the major-minor axis lengths for ideal ellipse were derived from two “normal” cross sections (immediately before and after the plaque region) using a decreasing factor to encompass vessel-narrowing along the segment length. The approximated ideal vessel boundary i.e. “stenosis-free” for the affected region is plotted in red contours of Fig. 3a - 3b. In the subsequent step, the annotated lumen (black contour) are subtracted from the ideal vessel (black contour) to compute stenosis grading precisely at particular location.

It is also important to mention here that the clinical threat associate with coronary stenosis is categorized into four levels depending upon the amount of plaque inside vessel and corresponding obstruction in the lumen. The four levels/grades for stenosis computation includes normal (minor plaque build-up with no significant impact on blood flow), mild, moderate and severe as detailed in Table 2. The table also defines total

Table 2

Cross Sectional dataset obtained from segmented coronary vasculature.

Plaque Type	Shrinkage %	Grading	Label	Cross-sectional slices
Non-calcified	$\leq 20\%$	Normal	0	7893
Non-calcified	20 - 49%	Mild	1	2412
Non-calcified	50 - 69%	Moderate	2	4149
Non-calcified	70 - 94%	Severe	3	1332
Non-calcified	$\geq 95\%$	Occluded	3	0
Total affected cross-sectional segments				15786

number of cross-sectional slices extracted in this research for respective grades. In general, severe and occluded categories are used in combination as there are rare annotations making obstruction greater than 94% and less than 100% explicitly.

4.3. Inter-observer variability

The performance of the stenosis grading algorithm is determined by comparing predicted stenosis grade with the manual expert based ground truth. To avoid biasing, the Rotterdam database provides vessel boundary demarcations from three independent. The vessel boundary demarcations were performed using exactly same environment to avoid any bias as the ultimate motive is to provide consistent reference contours to the end user for stenosis grading. Considering that lumen annotations were carried out by three different observers, a degree of inherent variability is anticipated. Thus, in this section, we conducted an analysis of inter-observer agreement to comprehend the discrepancies among observers.

An insight investigation of expert demarcations reveals that mutual agreement among three observers significantly relies on the importance of the segment. (proximal versus distal) and amount of plaque-buildup (mild versus severe) present. Typically, proximal segments exhibit increased brightness attributed to a higher concentration of the contrast medium in the blood, facilitating clear demarcations of the lumen boundary for human observers. Conversely, the distal segments present a more ambiguous appearance, making accurate demarcation of the lumen challenging. Additionally, the amount of the plaque (stenosis grade) also influences demarcations i.e. a severe plaque results in a substantial reduction of the lumen requiring greater effort of expert in demarcation, whereas a mild plaque induces a less pronounced compression of the lumen. This inter-observer disagreement is graphically

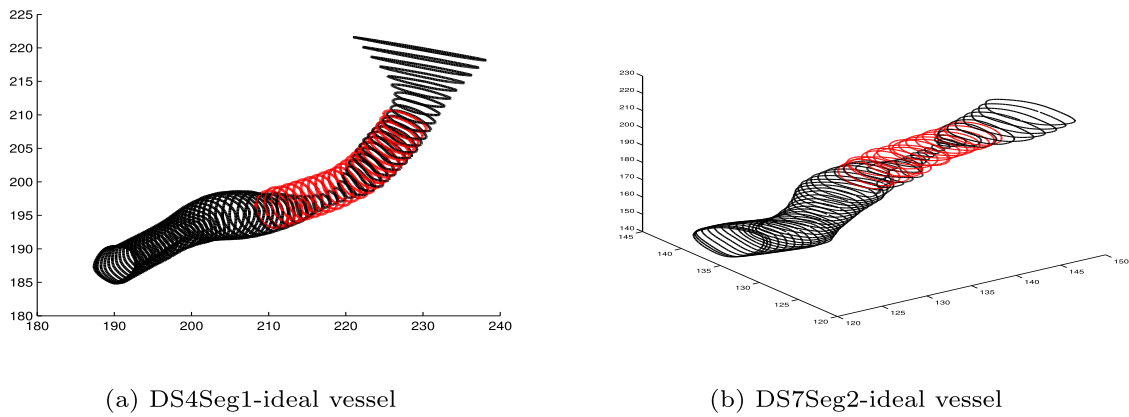


Fig. 3. Expert based lumen contours for two different segments. Manual expert-based vessel boundary contours are plotted using (black) whereas red contours define the “ideal” (plaque-free) boundary in the affected region constructed by contour interpolation in 3D space.

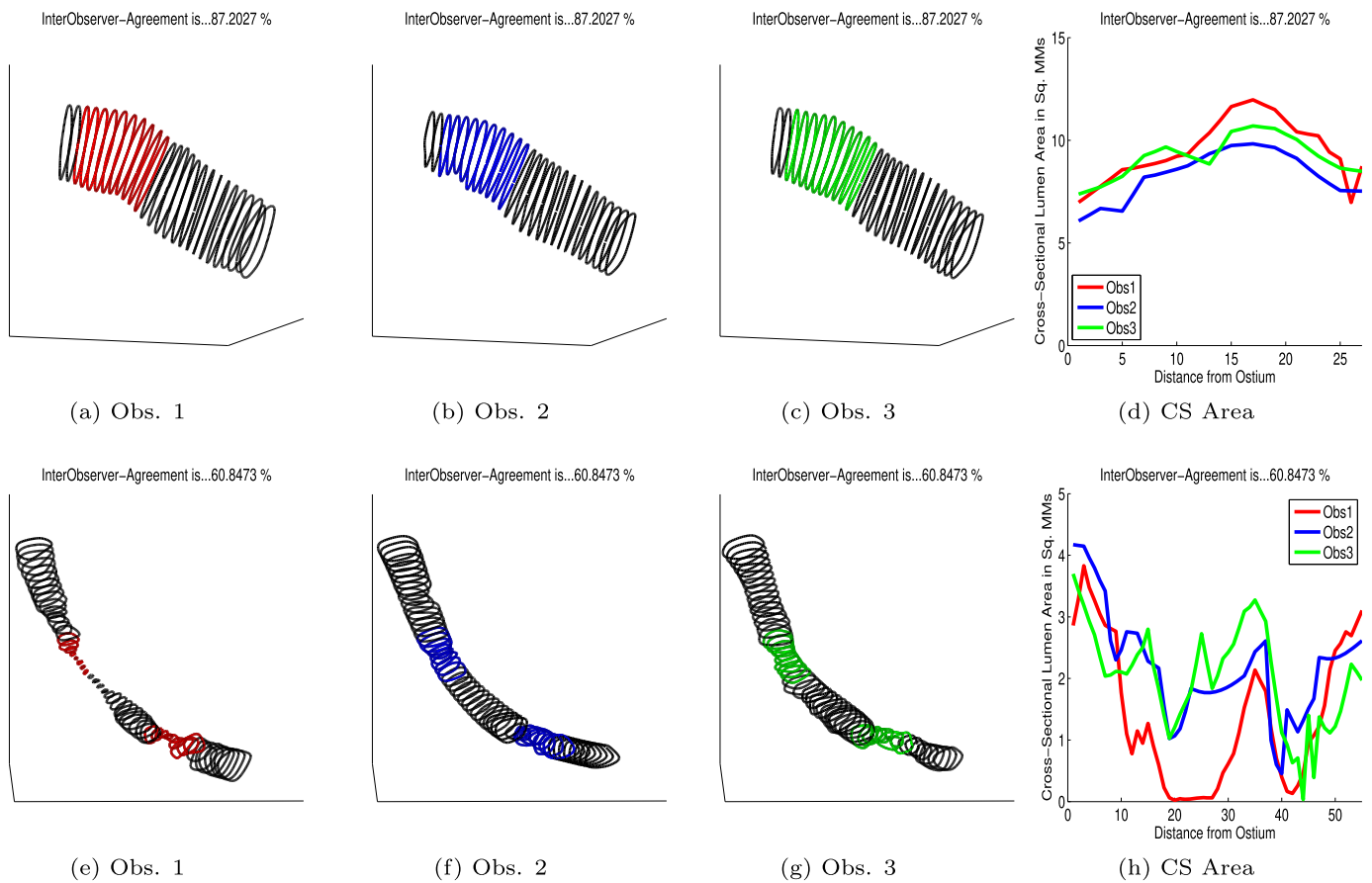


Fig. 4. Vessel demarcation for coronary segments by three manual experts. (a-c) reflects the lumen contours for segment having mild plaque with (d) showing a good mutual-agreement among three observers for lumen area. Likewise, (e-g) reflects lumen contours for segment having severe plaque with (d) showing substantial disagreement among three observers for lumen area.

demonstrated in Fig. 4, showing two cases i.e. a segment having a mild plaque (top row) versus a segment having a severe plaque (bottom row).

Fig. 4a - 4d represent the lumen contours for one proximal segment (DS1, segment 6) which has graded as “Mild” stenosis by manual experts. The top row shows tree lumen contours in black with colour annotations for plaque region by three independent observers respectively. Visually, it can be observed that all three observers exhibit a consistent trend, with no unexpected or abrupt deviations in the lumen boundary across the entire segment. Moreover, the mild nature of the plaque does not lead to any significant variation in observer’s reading; hence, the coloured contours (red, blue and green) shows a reasonable

overlap. This correlation of three observers is further investigated by investigating cross-sectional area (see Fig. 4d). It can be observed from Fig. 4d that the cross-sectional lumen area remains static and close to each other for three observers through out the length of the segment. In contrast, Fig. 4e - 4h represent the lumen demarcations for a segment suffering through severe stenosis. Accordingly, a significant variation in observer’s reading can be observed. One observer (red) annotates the lumen to a very narrow passage due to the severe plaque and difficulty to witness vessel in CT, whereas observer 2 and observer 3 have shown a reasonable lumen through the affected region of same patient. This disagreement also becomes apparent in the cross-section based area plot

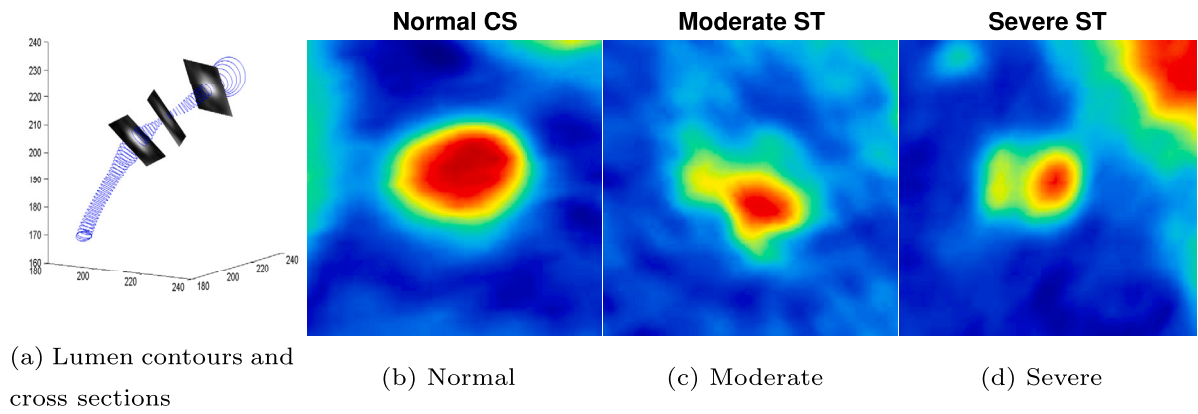


Fig. 5. Extraction of cross-sectional slices for individual segments. (a) shows cross sectional slices being extracted from 3D CT volume whereas (b-d) represents three respective cross-sections for normal moderate and severe plaque resulting in reduced lumen. It can be observed (b) that Normal cross section does have significant lumen surrounded by thin vessel-wall, (c) shows reduction in the lumen and (d) shows thick vessel-wall with very less lumen area.

Table 3

Jaccard overlap-based inter observer mutual agreement for two types of segment.

	Jaccard Measure	
	Mild Plaqued	Severe Plaqued
Expert (1) vs (2)	70.29	40.41
Expert (1) vs (3)	76.74	43.92
Expert (2) vs (3)	84.92	53.29

(see Fig. 4h) in which observer 1 based lumen area touches almost *zero* for the plaque-affected sections. In such cases, classification label is assigned to the segments using majority opinion of the experts as it is less likely for two individual experts to make mistake while performing lumen annotations.

This inter-observer variability allows a certain degree of freedom for the proposed stenosis-grading algorithm allowing results validation in a greater interval. From a statistical point of view, inter-observer mutual agreement for these coronary segments is presented in Table 3, which shows Jaccard overlap measure among three experts individually.

4.4. Cross section based stenosis grading

The extracted coronary tree as shown in Fig. 1a has been skeletonized using Fast marching method of [31] so that orthogonal cross section could be extracted for every segment of the coronary tree. The skeleton or the centreline (medial axis) is very important as it allows to track the true progression of the vessel in 3D space. Using centre line, orthogonal (“normal”) slices have been constructed throughout the length of the segment as demonstrated in Fig. 5a. Respective cross sections are also displayed in Fig. 5b - Fig. 5d for visual interpretation of normal, mild, moderate and severe plaque affected regions using customized colormap. It can be seen that Normal cross section does have significant lumen area (red) surrounded by vessel wall whereas corresponding degree of lumen reduction can be visualized in moderate and severe plaques respectively.

After obtaining the cross-sectional slices for respective segments of coronary tree, the subsequent step is to employ Convolutional Neural Network model for precise segregation of the plaque based on lumen reduction. Accordingly, we posed this as a four class problem as defined in Table 2. The proposed CNN model strategically employs the VGG16 architecture for image classification, leveraging its deep and expressive features. The choice of VGG16 over other pre-trained models is often influenced by its balance between model complexity and performance. VGG16 is known for its simplicity with a consistent convolutional kernel size (3x3) and deep stacking of layers, making it a

reliable choice for various computer vision tasks. The decision to use a pre-trained model i.e. VGG16, aligns with the concept of transfer learning i.e. using knowledge gained from solving one problem and applying it to a different but related problem. By leveraging pre-trained weights, the model has already learned hierarchical features using ImageNet, enabling it to recognize patterns, edges, and textures in images. This can significantly reduce the need for extensive labelled data and computational resources, making it practical for smaller datasets and research projects.

In the proposed model of Fig. 6, VGG16-base is used as seminal image feature extractor allowing extraction of useful spatial information from the convolutional layers. This freezing of pre-trained layers ensures that already learned features remain intact whereas the subsequent fully-connected layers are added to customize the model for specific classification task, promoting effective knowledge transfer. The proposed model extends beyond feature extraction and includes dense layers for classification. The added dense layers are responsible for learning high-level patterns and relationships in the features extracted by VGG16. These dense layers are trainable and specific to the custom classification task. The additional dense layers in the proposed introduce non-linearities and complexities to the model, allowing it to capture more intricate patterns and relationships specific to the target classification task. This flexibility can enhance the model’s ability to discriminate between different classes in the provided dataset. Moreover, these layers also allow for fine-tuning the model to the nuances of the custom dataset. The simulation has been performed for four-class lumen using “Adam” optimizer with custom-learning-rate = 0.001, Batch size of 32 and “Categorical-crossentropy” loss function with “accuracy” used as optimization metric. Moreover, out of the total 15786 cross-sectional images, a subset of 950 random images (belonging to all four classes) has been dedicated for test purpose whereas remaining images have been split into training/validation subsets using ratio of 80/20%.

Let X be the input tensor of shape $(224, 224, 3)$, and y be the predicted output for each class. The layers in the model are defined as follows:

Input Layer:

X (Input tensor of shape $(224, 224, 3)$)

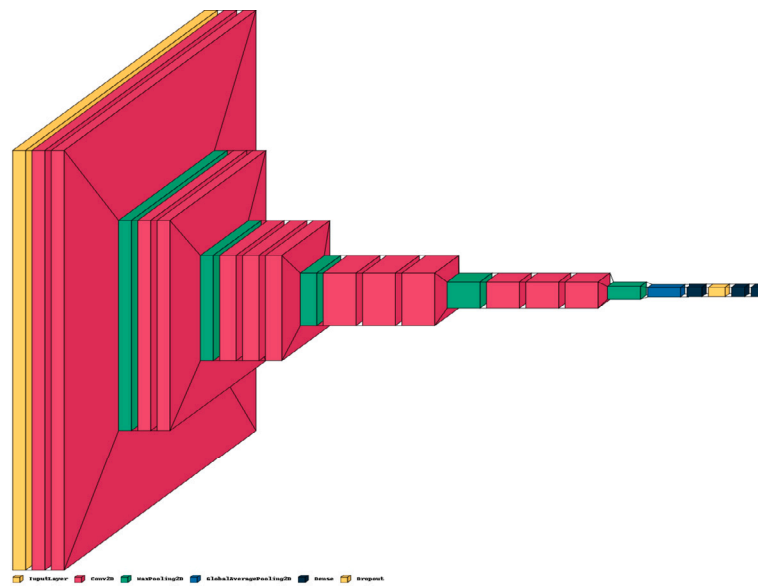
VGG16 Feature Extraction:

VGG16 layers with pre-trained weights up to Global Average Pooling

Global Average Pooling:

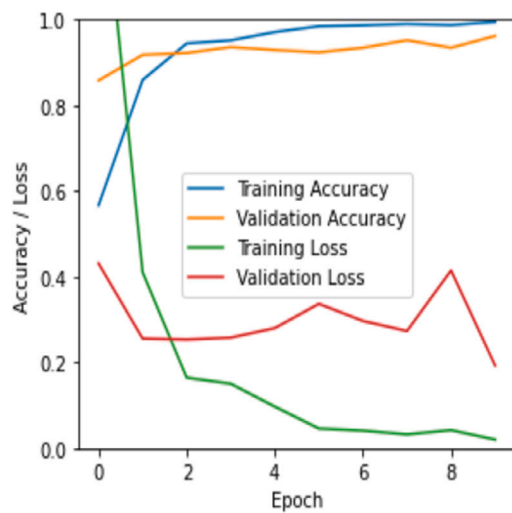
Average pooling operation to reduce spatial dimensions

Dense Layer 1:

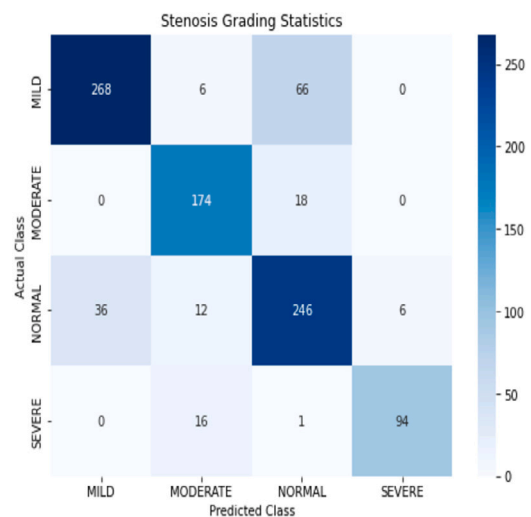


(a) Normal

Fig. 6. Customized CNN model for stenosis grading using customized 2D- cross sectional images from CT data. The appended fully-connected layers are used to capture and employ feature for stenosis quantification.



(a) Training and validation accuracy



(b) Confusion matrix

Fig. 7. Training performance and the confusion matrix statistics. The training for multi-class model shows that the accuracy improves with the passage of time whereas loss decreases as model keeps on learning. The confusion matrix overall represents the performance of stenosis grading model.

Dense layer with 256 units and ReLU activation
 Dropout Layer:
 Dropout layer with a dropout rate of 0.5
 Dense Layer 2:
 Dense layer with 128 units and ReLU activation
 Output Layer:
 y (Softmax activation with 4 units)
 The complete model, denoted as f_{my_model} , can be expressed as:

$$y = f_{my_model}(X)$$

The Performance of the model is visually represented using Fig. 7. It can be observed that both training and validation accuracy improves with the passage of time whereas the loss function shows a consistent decrease which validates the learning of the model.

5. Results

The performance of the proposed model has been evaluated in terms of capability to assign true stenosis grading labels to different coronary segments as per experts annotations. After training and validation of the customized model, model testing has been carried out on unseen test dataset (943 images). The model's predictions are generated for the test data subset, and the respective class labels are obtained using maximum probability prediction value. Subsequently, the predicted

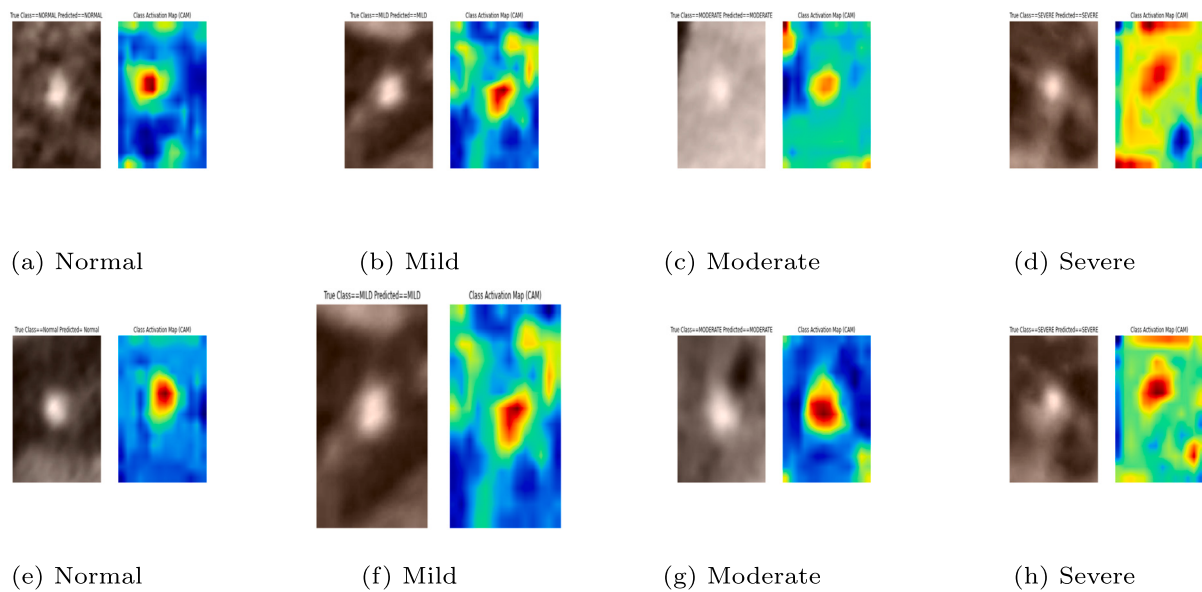


Fig. 8. Class activation maps (CAM) for four different classes. Column (1) shows activation map for two normal cross sections with three subsequent columns representing mild, moderate and severe plaque instances. It can be observed that the trained model concentrate upon the blood region and is well-capable to detect and assign true label as per stenosis grading.

class labels are compared with human expert-based manual labels for computing class-wise statistical metrics. The overall performance of the model is presented using confusion matrix of Fig. 7b where proper labels are assigned for comprehension. The grading performance of the model shows promising results with overall accuracy of 82.9%. Moreover, individual class-wise accuracy shows accuracy of 82% for Normal, 79% for Mild, 90.6% for Moderate and 85.4% for Severe stenosis. It can be observed that model is performing well for respective classes with a slight mis-classification in between “Normal” and “Mild” grades. This is due to the fact that small plaques (less than 20%) are normally ignored and segments are considered as normal manually whereas plaque in between 20%–49% is labelled as “Mild”. However, the model performs computations and due to close similarities between two grades, a number of “mild” cases are marked as “Normal”. Similarly, there are few cases of “Severe” category identified as “Moderate” due to the cut-off boundary between two classes. (Class activation map for respective classes is presented in Fig. 8.)

5.1. Vessel wall analysis

In order to validate the findings of our model i.e. whether true degree of the stenosis has been assigned, we manually performed investigation for lumen-area versus vessel-wall thickness for 2D cross sections. Accordingly, voxel-wise classification was performed in the segmented coronary tree using 3-class Gaussian Mixture Model (GMM) [32] to separate the background, vessel-wall and the lumen. The proposed 3-class GMM is based on the assumption that low-intensity based non-calcified plaque will lead to reduced lumen and expanded vessel wall. Subsequently, GMM was followed by Bayesian Posterior probability computation to group voxels into three categories respectively as illustrated in Fig. 9. The first column represents two cross-sectional slices from segmented coronary tree with 6 mm expansion to ensure that maximum possible expansion could be captured, the second column represents the background included in 6 mm expansion whereas vessel wall and corresponding lumen are presented in third and fourth column respectively. It can be observed from the second column of the Fig. 9 that low-intensity based surrounding/background included in segmented tree is well identified by “class-1”, the vessel-wall is very reasonable captured by “class-2” of GMM and class-3 representing the lumen is shown in column 4.

In the instance of a cross-section affected by plaque (bottom row), the 3-class approximation precisely depicts abnormalities in both the lumen and the vessel wall. Given that non-calcified plaque typically exhibits intensity values lower than the blood lumen and much similar to myocardial tissues, the 3-class approximation designates “Plaque voxels” to “class-2” representing the expanded/thick vessel wall. Consequently, an extra thick vessel-wall with reduced lumen is displayed for abnormal segment in the bottom row.

After extracting the vessel wall, the statistical thickness measure for vessel-wall was computed using ray-projection method as depicted in Fig. 10a–10b. Starting from the centre of the lumen, we projected a total of 36 rays outward with an angular interval of 10 degrees. The thickness of the vessel wall was computed individually for each ray and then averaged to determine the overall wall thickness for the respective cross-section. The subsequent, wall thickness plots for two plaque affected segments as shown in Fig. 11a–11b.

It can be observed that for both segments, the lumen area (black) starts with sharp decrement and becomes stable as we move away from the aorta. Similarly, the wall thickness (red) shows a stable thickness value for normal region of the segment. However, in the region affected by plaque, an unexpected reduction in lumen and an unanticipated increase in wall thickness can be observed. Along with the qualitative analysis of Fig. 11, quantitative analysis performed for different segments also validates the performance of the proposed model as represented in Table 4.

6. Discussion

In this work, we proposed a method for computation of coronary stenosis and subsequent grading into four categories according to the severity of the problem. We started with segmentation of coronary tree from CT using [27]. In the subsequent step, non-calcified plaque was detected and localized using [30]. After validation of plaque position with the manual reference of Table 1, severity based plaque labelling was performed using clinical practice. According based upon lumen-narrowing percent, four labels were derived namely Normal, Mild, Moderate and Severe. In the subsequent stage, CNN model was employed to perform four-class classification and results were validated with respect to manual ground truth.

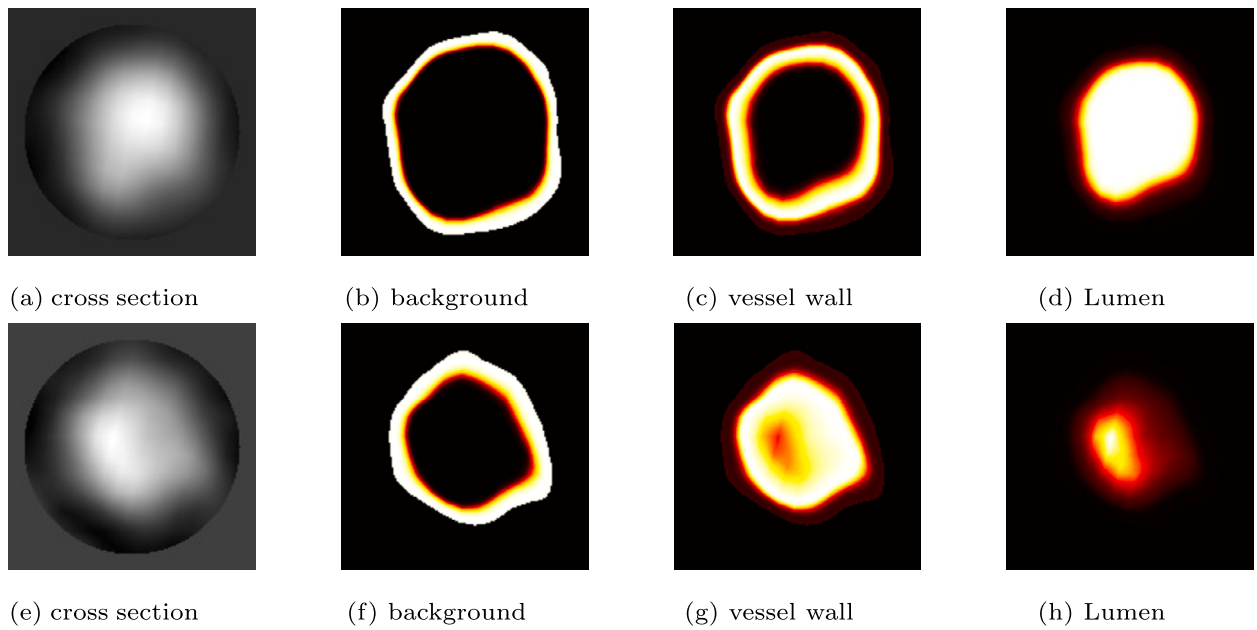


Fig. 9. Vessel-wall thickness using 3-class GMM for normal segment 9 (top row) and abnormal segment (bottom row). The first column represents maximum expansion for coronary using 6 mm surrounding, second column shows the background separation and last two columns shows wall and lumen respectively.

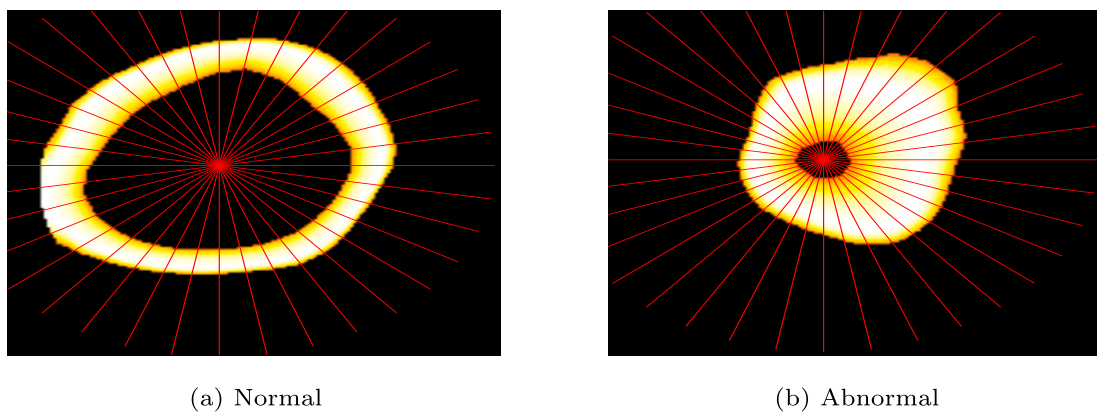


Fig. 10. Wall thickness using angular ray-projection for two cross-sectionals slices. (a) represents normal leading to normal vessel wall measurement, whereas abnormal cross section (b) lead to expansion of the vessel wall based on low density soft plaques.

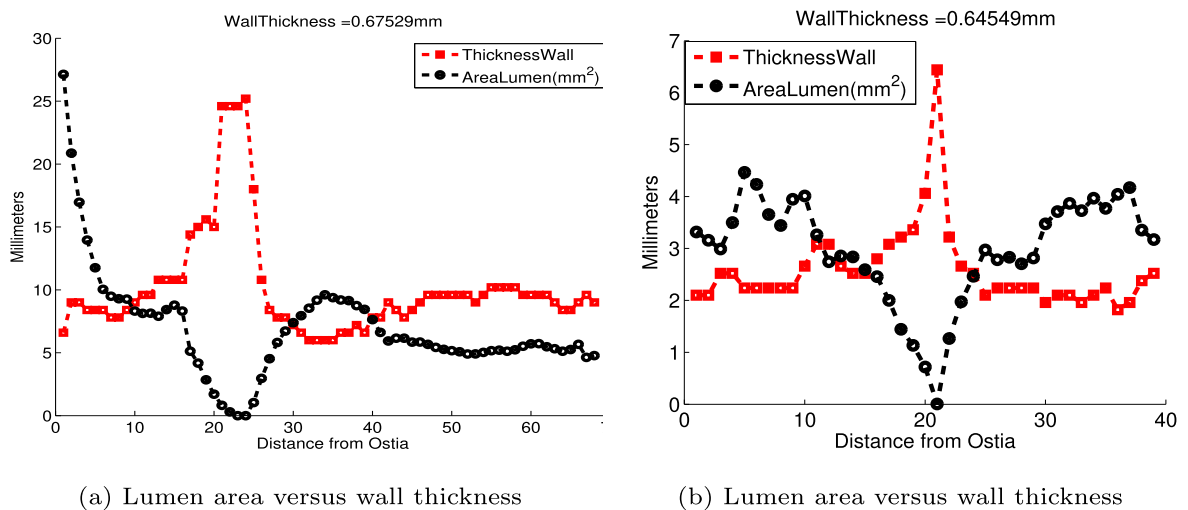


Fig. 11. Lumen shrinkage versus vessel-wall expansion for abnormal segments. It can be observed graphically that non-calcified plaque based vessel wall expansion leads to compression of lumen at certain points along the length of the segment.

Table 4
Segment wise stenosis computation.

	Lumen reduction based Stenosis				Reference Groundtruth	
	Ideal Area	Actual Area	Red%	Stenosis grade	Ref Red%	Ref Grade
DS2 Seg6	4.5	3.2	29	Mild	25	Mild
DS4 Seg1	9	0.5	93	Severe	95	Severe
DS7 Seg3	2.9	0.5	82	Severe	81	Severe
DS9 Seg2	7.5	3.3	55	Moderate	65	Moderate
DS11 Seg7	4.2	3.1	25	Mild	32	Mild
DS15 Seg2	6.8	3.7	45	Mild	53	Moderate

It is important to mention that stenosis related to non-calcified plaques is always challenging due to ambiguous visual behaviour of plaques in CT. Accordingly, the proposed method employed a mix of classical image processing with machine learning to precisely detect and grade the threat with a good agreement to human experts. The CT data and respective manual annotations were obtained from Rotterdam Coronary Artery platform and the results are compared with expert annotations. The proposed method shows good agreement with human experts as well as inline with the Non-Calcified plaque assessment methods work [33,34,24]. The qualitative and statistical results demonstrate the applicability of the proposed method and which can be further extended by involving clinical collaborator in future. Moreover, GMM-based findings for vessel-wall expansion and lumen reduction can be integrated in conventional ML methods for stenosis grading and performance comparison with CNN approach.

Declaration of competing interest

None declared.

Acknowledgement

We acknowledge the support of our clinical partner Dr. Ronak Rajani from Guys & St. Thomas Hospital, London for provision of the CTA data, his interest and valuable guidance throughout this research. Moreover this work has been carried out as a part of PhD and no explicit funding has been received. Furthermore, this research does not require the ethical approval as we received past anonymized CT data from Rotterdam Coronary Artery Framework website [28].

References

- [1] B. H. Foundation. Global heart & circulatory diseases, factsheet. Available at [https://www.bhf.org.uk\(2023/12/07\)](https://www.bhf.org.uk(2023/12/07)), 2024.
- [2] Flohr T, Ohnesorge B. Multi-slice ct technology. In: Multi-slice and dual-source CT in cardiac imaging. Springer; 2007. p. 41–69.
- [3] W. H. Organization. Cardiovascular diseases CVDs, the global statistics. Available at [http://www.who.int/mediacentre/factsheets/fs317/en/\(2023/12/07\)](http://www.who.int/mediacentre/factsheets/fs317/en/(2023/12/07)).
- [4] David MS, Levin C, Fischman D. Coronary CTA, a cost-effective alternative to cardiac catheterization for the evaluation of cad, study suggests. Available at [https://www.sciencedaily.com/releases/2010/04/100421162617.htm\(2023/12/07\)](https://www.sciencedaily.com/releases/2010/04/100421162617.htm(2023/12/07)).
- [5] Saur SC, Alkadhi H, Desbiolles L, Székely G, Cattin PC. Automatic detection of calcified coronary plaques in computed tomography data sets. In: International conference on medical image computing and computer-assisted intervention. Springer; 2008. p. 170–7.
- [6] Brunner G, Kurkure U, Chittajallu DR, Yalamanchili RP, Kakadiaris IA. Toward unsupervised classification of calcified arterial lesions. In: International conference on medical image computing and computer-assisted intervention. Springer; 2008. p. 144–52.
- [7] Išgum I, Rutten A, Prokop M, van Ginneken B. Detection of coronary calcifications from computed tomography scans for automated risk assessment of coronary artery disease. Med Phys 2007;34(4):1450–61.
- [8] Mohr B, Masood S, Plakas C. Accurate lumen segmentation and stenosis detection and quantification in coronary cta. In: Proceedings of 3D cardiovascular imaging: a MICCAI segmentation challenge workshop; 2012.
- [9] Virmani R, Burke AP, Farb A, Kolodgie FD. Pathology of the vulnerable plaque. J Am Coll Cardiol 2006;47(8s1):C13–8.
- [10] Waxman S, Ishibashi F, Muller JE. Detection and treatment of vulnerable plaques and vulnerable patients novel approaches to prevention of coronary events. Circulation 2006;114(22):2390–411.
- [11] Clouse ME, Sabir A, Yam C-S, Yoshimura N, Lin S, Welty F, et al. Measuring non-calcified coronary atherosclerotic plaque using voxel analysis with mdct angiography: a pilot clinical study. Am J Roentgenol 2008;190(6):1553–60.
- [12] Wei J, Zhou C, Chan H-P, Chughtai A, Agarwal P, Kuriakose J, et al. Computerized detection of noncalcified plaques in coronary ct angiography: evaluation of topological soft gradient prescreening method and luminal analysis. Med Phys 2014;41(8):081901.
- [13] Renard F, Yang Y. Image analysis for detection of coronary artery soft plaques in mdct images. In: 2008 5th IEEE international symposium on biomedical imaging: from nano to macro. IEEE; 2008. p. 25–8.
- [14] Tessmann M, Vega-Higuera F, Fritz D, Scheuring M, Greiner G. Multi-scale feature extraction for learning-based classification of coronary artery stenosis. In: SPIE medical imaging, international society for optics and photonics; 2009:726002.
- [15] Brodoefel H, Burgstahler C, Heuschmid M, Reimann A, Khosa F, Kopp A, et al. Accuracy of dual-source ct in the characterisation of non-calcified plaque: use of a colour-coded analysis compared with virtual histology intravascular ultrasound. Br J Radiol 2009;82(982):805–12.
- [16] Zuluaga MA, Magnin IE, Hoyos MH, Leyton EJD, Lozano F, Orkisz M. Automatic detection of abnormal vascular cross-sections based on density level detection and support vector machines. Int J Comput Assisted Radiol Surg 2011;6(2):163–74.
- [17] Athanasiou L, Rigas G, Sakellarios AI, Exarchos TP, Siogkas PK, Bourantas CV, et al. Three-dimensional reconstruction of coronary arteries and plaque morphology using ct angiography—comparison and registration with ivus. BMC Med Imaging 2016;16(1):9.
- [18] Sun Z, Xu L. Coronary ct angiography in the quantitative assessment of coronary plaques. BioMed Res Int 2014. <https://doi.org/10.1155/2014/346380>.
- [19] Schepis T, Marwan M, Pfloderer T, Seltmann M, Ropers D, Daniel WG, et al. Quantification of non-calcified coronary atherosclerotic plaques with dual-source computed tomography: comparison with intravascular ultrasound. Heart 2010;96(8):610–5.
- [20] Dey D, Schepis T, Marwan M, Slomka PJ, Berman DS, Achenbach S. Automated three-dimensional quantification of noncalcified coronary plaque from coronary ct angiography: comparison with intravascular us. Radiology 2010;257(2):516–22.
- [21] Pfloderer T, Schmid M, Ropers D, Ropers U, Komatsu S, Daniel W, et al. Inter-observer variability of 64-slice computed tomography for the quantification of non-calcified coronary atherosclerotic plaque. In: RÖFo-Fortschritte auf dem Gebiet der Röntgenstrahlen und der bildgebenden Verfahren, vol. 179. New York: Georg Thieme Verlag KG Stuttgart; 2007. p. 953–7.
- [22] Otsuka M, Bruining N, Van Pelt NC, Mollet NR, Ligthart JM, Vourvouri E, et al. Quantification of coronary plaque by 64-slice computed tomography: a comparison with quantitative intracoronary ultrasound. Invest Radiol 2008;43(5):314–21.
- [23] Schlett CL, Ferencik M, Celeng C, Maurovich-Horvat P, Scheffel H, Stolzmann P, et al. How to assess non-calcified plaque in ct angiography: delineation methods affect diagnostic accuracy of low-attenuation plaque by ct for lipid-core plaque in histology. Eur Heart J—Cardiovasc Imag 2013;14(11):1099–105.
- [24] Han D, Liu J, Sun Z, Cui Y, He Y, Yang Z. Deep learning analysis in coronary computed tomographic angiography imaging for the assessment of patients with coronary artery stenosis. Comput Methods Programs Biomed 2020;196:105651.
- [25] Paul J-F, Rohnean A, Giroussens H, Pressat-Laffouilhère T, Wong T. Evaluation of a deep learning model on coronary ct angiography for automatic stenosis detection. Diagn Interv Imaging 2022;103(6):316–23.
- [26] Jin X, Li Y, Yan F, Liu Y, Zhang X, Li T, et al. Automatic coronary plaque detection, classification, and stenosis grading using deep learning and radiomics on computed tomography angiography images: a multi-center multi-vendor study. Eur Radiol 2022;32(8):5276–86.
- [27] Jawaid MM, Rajani R, Liatsis P, Reyes-Aldasoro CC, Slabaugh G. A hybrid energy model for region based curve evolution-application to cta coronary segmentation. Comput Methods Programs Biomed 2017;144C:189–202.
- [28] Theo W. The great challenge, coronary artery stenoses detection and quantification evaluation framework. <http://www.http://coronary.bigr.nl/stenoses/>, 2016.
- [29] Kirişli H, Schaap M, Metz C, Dharampal A, Meijboom WB, Papadopoulou S-L, et al. Standardized evaluation framework for evaluating coronary artery stenosis detection, stenosis quantification and lumen segmentation algorithms in computed tomography angiography. Med Image Anal 2013;17(8):859–76.

- [30] Jawaid MM, Riaz A, Rajani R, Reyes-Aldasoro CC, Slabaugh G. Framework for detection and localization of coronary non-calcified plaques in cardiac cta using mean radial profiles. *Comput Biol Med* 2017;89(C):84–95.
- [31] Van Uiter R, Bitter I. Subvoxel precise skeletons of volumetric data based on fast marching methods. *Med Phys* 2007;34(2):627–38.
- [32] Reynolds DA, et al. Gaussian mixture models. *Encyclopedia of biometrics*, vol. 741. 2009. p. 659–63.
- [33] Song F-X, Zhou J, Zhou J-J, Shi Y-X, Zeng M-S, Zhang Z-Y, et al. The diagnosis of coronary plaque stability by multi-slice computed tomography coronary angiography. *J Thorac Dis* 2018;10(4):2365.
- [34] Kolossvary M, Szilveszter B, Merkely B, Maurovich-Horvat P. Plaque imaging with CT—a comprehensive review on coronary CT angiography based risk assessment. *Cardiovasc Diagn Ther* 2017;7(5). <http://cdt.amegroups.com/article/view/14282>.